Flowpattern in hydrocyclones, numerical simulations with experimental verification

Flowpattern in hydrocyclones, numerical simulations with experimental verification

Alex C. Hoffmann[1], Daniel Fonnes[1] and Yu-Fen Chang[1,2,3]

[1] Dept. of Physics and Technology, University of Bergen, Allégaten 55, 5007 Bergen, Norway
[2] Western Norway University of Applied Sciences, Inndalsveien 28, 5063 Bergen, Norway
[3] UiT The Arctic University of Norway, Hansine Hansens veg 18, 9019 Tromsø Norway

E-mail: alex.hoffmann@uib.no, yu-fen.chang@hvl.no, yu-fen.chang@uit.no

Abstract. This paper reports a detailed study of the flow in cyclone separators, with the use of most up to date computational fluid dynamics simulations, which are validated with positron emission particle tracking (PEPT) experiments tracing the movement of particles through the cyclone. The parameters varied were the viscosity of the carrier liquid, the flowrate and, in the numerical simulations, the inlet configurations of the cyclone, namely one and two inlets and, with the two inlets, a) both at right angles to the cyclone axis and b) angled downwards. The study reveals features of the flow, which have not been seen till now, but are necessary for the understanding and modelling of the separation and purification efficiency of cyclones. The results of the simulations and the close agreement with experiment are a testament to the reliability and accuracy of large eddy simulation (LES), even for flow features as difficult to simulate as the confined strongly swirling flows in cyclone separators. The results show that a contiguous, smooth surface of zero axial velocity does exist and has approximately the shape that has been assumed by modellers. The significant effects of fluid viscosity, underflow and modifications to the inlet are also shown.

1. Introduction

Cyclones are used in many important industries as separators to separate solids from fluids, to separate immiscible fluids of different densities and as classifiers to increase or decrease dispersed phase concentrations in multiphase mixtures. Cyclones can also be used for classification of solid particles according to size or density.

They are very widely used as the first and most important step in the cleaning of gaseous or liquid effluents before discharge to the environment, whether the atmosphere or the sea, and knowledge-based design and optimisation of cyclones is therefore of interest to the technological and scientific community, as also evidenced by the large number of recent articles cited in this article.

The focus of this work is on solid-liquid separation, the relevance of which is increasing, especially in the petroleum industry. As the reserves of oil and gas are declining, reserves that previously have been seen as non-commercial due to technological limitations or the cost of extracting and/or processing have now become feasible. Mature oilfields are also producing for a longer time, which presents new challenges due to increased water and sand production. To meet these challenges it is important to know the limitation of the equipment and to ensure that equipment can meet the needed specifications. The move to subsea processing, which

allows processing and purification under pressure and makes it possible to limit the material that needs to be transported to the surface also makes it more critical to know the performance of processing equipment precisely, so that intervention in subsea installations, which is costly and time consuming, can be minimised.

The simplicity, robustness and compactness of the cyclone are key properties explaining its extensive use. Though simple in construction, the complex internal flow of the cyclone has been a focus of intensive research using state-of-the-art computational and experimental techniques. A challenge has been to produce good experimental results for the details of the flow pattern of the fluid and the particles inside the cyclone. The approach in this work is to use positron emission particle tracking (PEPT) to extract the trajectory of an actual particle as it moves through the cyclone. This is made possible by the use a positron emission tomography (PET) scanner and a mobile flow loop in which the cyclone is installed, and a positron emitting ion-exchange resin tracer particle.

The primary aim of this project is to improve the understanding of solid-liquid separation in the cyclones, focusing on the flow features controlling the particles' actual paths through the cyclone and their separation/capture or emission/loss from the cyclone, also to throw light on the most successful models prediction cyclone separation performance. Recent technological advances in PEPT have made possible tracking of an individual particle at high velocity with the required accuracy to explicitly reveal the particle trajectory through a cyclone. The tracking of individual particles experimentally reveals how the cyclone is performing and where any trouble areas are located. This work combines the results from PEPT experiments with numerical simulation of an identical setup. Being able to regenerate simulated trajectories qualitatively similar to the PEPT trajectories, this is strong evidence that the numerical simulations are valid and can be used in the further investigation of the flow pattern inside the cyclone.

1.1. Modelling

We review here briefly some of the important features and basic assumptions of the most successful cyclone separation performance models, which will be relevant to the work described in this paper. It is fair to say that the most used cyclone separation models are based on the 'equilibrium orbit' concepts pioneered by Walter Barth [1] and later developed further by Muschelknautz [2], Mothes and Löffler [3], Lorenz [4] and Muschelknautz [5], among others.

The equilibrium-orbit models are based on the concept that the axial flow direction in the outer part of the vortex in reverse-flow cyclones is downwards in the direction of the dust outlet and the axial flow in the inner part of the vortex is upwardly directed, towards the fluid outlet. A particle in the outer part of the vortex will therefore be separated, while one in the inner part will be lost and emitted from the cyclone. A surface of zero axial velocity separates the two regions, and the particle rotating in this surface (in this paper called CS for 'control surface', sometimes called LZVV for 'locus of zero vertical velocity' [6]) will be lost or separated with equal probability, and is therefore the cyclone 'cut size'. The forces acting on the particle rotating in CS are:

- A radially inwardly directed drag force due to the flow across CS (this flow is assumed to be uniform) of the carrier fluid as it moves from the radius of the inlet to that of the carrier fluid outlet
- The outwardly directed 'centrifugal force' due to the rotation of the particle

For the cut size these two are equal.

The question arises where this surface of zero vertical velocity is located. Most assume this surface to be the cylindrical surface obtained by prolonging the vortex finder tube to the bottom of the cyclone, while some, most notably Svarovsky [6], assumed it to be a conical surface ('mantle') with the base at the lower cross-section of the vortex finder and the apex at

the bottom of the cyclone. The latter has often been used in the modelling of hydrocyclones, and the former for gas cyclones, although there is no fundamental reason there should be a difference in this respect between the two, at least in the absence of a gas core in the hydrocyclone. This question will be answered by the results presented in this paper.

A large number of papers have been published wherein these models are discussed and used for cyclone performance modelling, some recent ones are refs [5, 7–17]

Although it is still such that the classical analytical cyclone cut-size models are the most successful and the most used for predicting cyclone performance, the trend both in the research literature and in industry has been to model cyclones using computational fluid dynamics (CFD). This was for a long time fraught with difficulties, since it turned out that the classical turbulence models, such as the $k-\epsilon$ model, could not be used for modelling the strongly swirling confined flows in cyclones. However, more advanced turbulence models, such as the Reynolds Stress model (RSM) and the large eddy simulation (LES) turbulence model proved to be suitable for the simulation of the flow in cyclones, and this has made CFD simulation of cyclones very popular. Gronald and Derksen [18] reviewed this issue and some papers discussing the simulation of the flow in cyclones by CFD using the latest turbulence models are refs [7, 10, 11, 19–29]. The major CFD packages even offer a cyclone as a standard test case for new users. Mousavian and Najafi [30] found that LES simulations were superior to other turbulence models in simulating the flow in cyclones. In CFD simulations, the number of grid points required to directly resolve all turbulent scales scales with Re^3, limiting the practicality for very high-Re flows. In LES, the large eddies are explicitly resolved on the grid, while the smaller eddies are modelled using subgrid-scale (SGS) models that account for the turbulent energy transfer from the large to the small scales. Using LES and SGS models makes it possible to capture the essential features of turbulence at a lower computational cost compared to direct numerical simulation (DNS). In this study, the Reynolds numbers are above 3500, except for the tests with the highest viscosity (20 cP) [31]. Using LES and SGS models strikes a balance between capturing the important large-scale features of turbulence and modelling the effects of the small, unresolved scales, making it possible to study turbulent flows in a computationally efficient manner.

The dynamics of particles in cyclones is normally simulated by Lagrangian particle tracking. Tracking enough particles of varying sizes till they leave the cyclone, either through the dust exit (collected) or the carrier fluid exit (lost), will yield a grade-efficiency curve and thus a cut-size as the size of particle that will be collected with 50% efficiency. Eulerian modelling of the particle flow has not been published much, even though this would elucidate important phenomena taking place in cyclones and make easier the simulation of flow features caused by the effects of two-way coupling, which is especially important in the region just after the inlet.

1.2. PEPT

The experimental method for validating the CFD simulations is positron emission particle tracking (PEPT). This method, which was pioneered in Birmingham UK by Seville and Parker [32–35], makes it possible to track a particle moving through a process, located in the field of view (FOV) of a three-dimensional (3D) detector array, by cross-triangulation. The method is based on the radioactive decay of a suitable isotope with which a tracer particle is labelled, in the work shown here $^{18}\mathrm{F}$, which gives rise to the emission of a positron that travels some small distance through the medium till it annihilates with an electron giving rise to the back-to-back emission of two photons of 511 keV each. These photons are detected by detectors and a straight line between two detectors reacting to the same annihilation event (i.e. both within a very narrow time window) defines a 'line of response' (LOR), somewhere along which the annihilation event must have taken place. Cross triangulation using many LORs within a short time interval allows determination of the centroid of the tracer particle, the accuracy of which depends on the cross-triangulation algorithm and the activity on the tracer particle.

Some scatter is inherent in the process, the reasons for this are discussed in refs [36] and [37] and are briefly listed below:

- The length through which the emitted positron travels before annihilation
- The angle between the two photons may be less than 180 degrees, due to the positron and electron annihilating having significant amounts of kinetic energy
- The photons emitted may be deflected due to interaction with the material (Compton scattering) on their way to the detectors
- Three photons may be generated in one annihilation, or one photon from each of two annihilation events occurring at the same time may be detected, giving rise to false LORs
- 'Parallax blurring' occurs if a photon impacts obliquely on and penetrates a detector, and is detected by the neighbouring detector

The authors of this paper have developed accurate algorithms for determining the particle position, and this, combined with efficient particle labelling, has made it possible to locate the particle centroid with a standard deviation of less than 100 μm in all three coordinate directions. The most reliable way of estimating the standard deviation in the ms positions (meaning that one position is determined every millisecond) of the tracer particle centroid is to determine the position of a stationary particle. In the context of another project, such a determination was carried out, and the standard deviations in six series, each consisting of 1000 ms positions were determined. The mean standard deviations in the positions of the centroid of the tracer particle were 93.51 ± 0.648, 86.51 ± 0.299 and 80.97 ± 0.810 μm in the x, y and z-directions, respectively, where the z axis is the axis aligned with the axis of the cylindrical field of view of the PET scanner. This is much better accuracy than any reported in the published literature [38]. This very high spatial resolution is also evident in the results published in this paper. The standard deviation scales with $1/\sqrt{n}$, where n is the number of LORs used in the cross-triangulation [21, 39].

The algorithm developed by the authors is based on using the analytical expression for the spatial point that minimises the sum of squares of the distances to all the LORs measured within one millisecond as a first approximation, and then considering LOR cutpoints in the plane normal to the z-axis (the x-y plane) in a series of iterative steps, in each step eliminating LORs with only outlying cutpoints in successively narrower spatial windows, the final window size chosen as the one leading to the smallest scatter in the millisecond positions. For the positioning in the y-z plane, only the LORs remaining after the elimination process in the x-y plane are included. This algorithm used in this work can be applied to track multiple particles at a time if the differences between the radioactivity of each particle are adequate. Algorithms on basis of fitting the cutpoint distribution with peak shape functions as well as computing the 3D relations between LORs have been developed in our lab for tracking single and multiple particles. Other algorithms for tracking of multiple particles simultaneously, on basis of density maps for the LORs [40], on basis of machine learning [41] and on basis of identifying voxels with many LOR crossings [39], have been developed. The algorithm used in this paper is illustrated in Figure 1.

Work in various groups is also ongoing to develop new tracer particles, some recent papers discussing or reviewing this are refs [42–47].

2. Scope and Objectives of this work

This work is part of a larger project aimed at determining the suitability of cyclone separators for separating a variety of solids from liquid streams consisting of liquids other than water, focusing on liquids of higher viscosity than that of water.

The specific aims of the work described in this paper are to verify that numerical simulations of the fluid and particle flows can correctly reflect even the unsteady and unstable phenomena

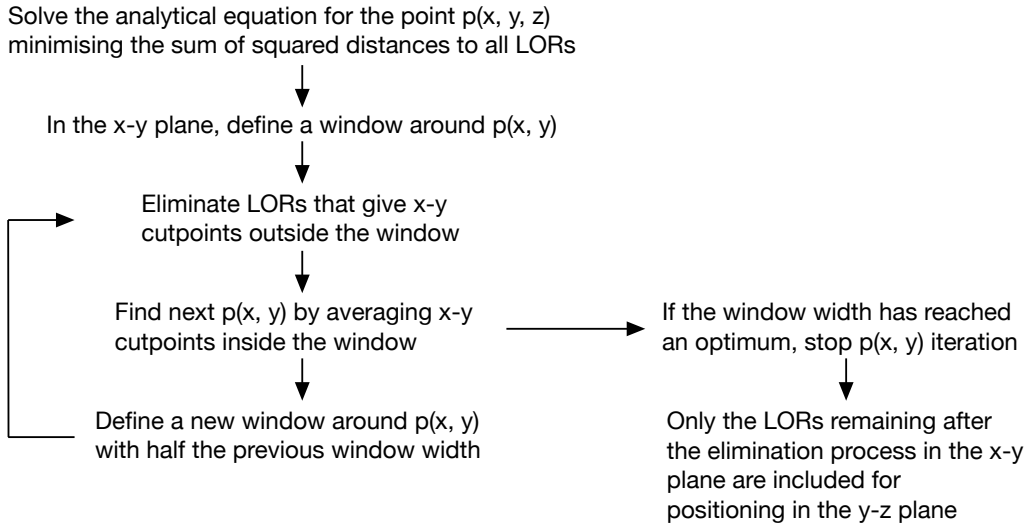

Figure 1. Figure outlining the structure of the PEPT particle positioning algorithm used in this work developed by the authors.

taking place. Furthermore to use numerical simulations to elucidate some of the important assumptions on which the most utilised and successful analytical cyclone performance models are based.

3. Simulations and experiments

A brief account of the numerical simulations and experiments carried out during this work will be given in in this section.

The CFD simulations in this work are performed with the LES turbulence model and the Smagorinsky subgrid turbulence model, which in previous work has proven to be the model most accurately reflecting experimental results [48]. We note that also the RSM model gave results qualitatively agreeing with experiment.

The equations to be solved numerically are the Navier-Stokes equations:

$$\begin{aligned} \boldsymbol{\nabla} \cdot \mathbf{v} &= 0 \\ \rho \frac{D\mathbf{v}}{Dt} &= \rho \mathbf{g} - \boldsymbol{\nabla} p + \mu \boldsymbol{\nabla}^2 \mathbf{v} \end{aligned} \tag{1}$$

A numerical mesh is applied to cover the domain of interest, and discrete representations of the equations are solved on the mesh. The mesh has to be fine enough to obtain an accurate solution, and as coarse as possible to limit the computational effort.

For LES of the flow of incompressible fluids a spatial filter is applied to the flow variables. For an arbitrary flow variable, $\phi(\mathbf{x})$, which could be a component of the fluid velocity or the pressure, the spatial filter is:

$$\bar{\phi} = \int G(\mathbf{x} - \mathbf{x}', \Delta) \phi(\mathbf{x}', t) d\mathbf{x}' \tag{2}$$

where $G(\mathbf{x}, \Delta)$ is some suitable function of the spatial coordinates. Δ is the width of the filter, similar in magnitude to the size of the computational cells. By applying this filter, turbulent eddies smaller than the grid size are filtered out, and their effect on the flow is modelled with

a subgrid turbulence model. This model, however, can be much simpler than most turbulence models in use, since this fine-scale turbulence is almost isotropic. In this work the well-known and very simple Smagorinsky subgrid turbulence model was used. The larger eddies are in LES simulated directly.

The geometry of the cyclone, which is the same as that used in the experiments, is shown in Figure 2A, and details of the numerical grid are shown in Figure 2B. A 'trimmer' model is used for the grid together with a Prism layer mesher and Surface remesher. The number of prism layers is two and the base size of the grid-cells is 1.2 mm. To check for grid independence several simulation cases were run with the base size varying from 0.8 to 2.0 mm with increments of 0.2 mm. From this, a base size of 1.2 mm was found to be acceptable. For the Lagrangian particle tracking the drag model of Schiller-Naumann was used. More details about the numerical simulation scheme are given in ref [49]. The simulations were performed using the software package Star-CCM+. This work builds on the work described in [49], but since that work the cyclone used for the experiments has been significantly improved in order to more closely match the geometry used in the CFD simulations. The inlet was modified to make it better match that of a standard slot-inlet cyclone and the CFD geometry. In addition to the modification to the inlet, also the wall of the vortex finder tube was made thinner. Some modifications to the flow loop were also made to avoid vibrations and improve the flow from the holding tank and the flows in the pump and through the cyclone underflow.

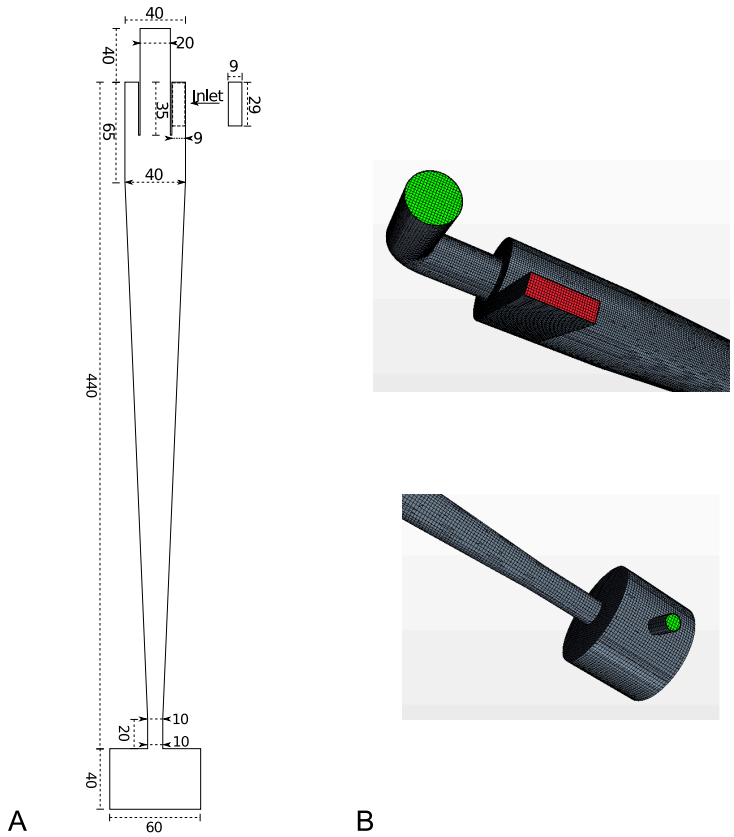

Figure 2. The cyclone used in the experiments and the simulations. A) The geometry of the cyclone, drawn to scale. The dimensions are given in mm. B) Details of the numerical grid used in the CFD simulations.

The experimental rig is shown in Figure 3, in diagrammatic form in Figure 3A and installed

in the PET scanner in Figure 3B.

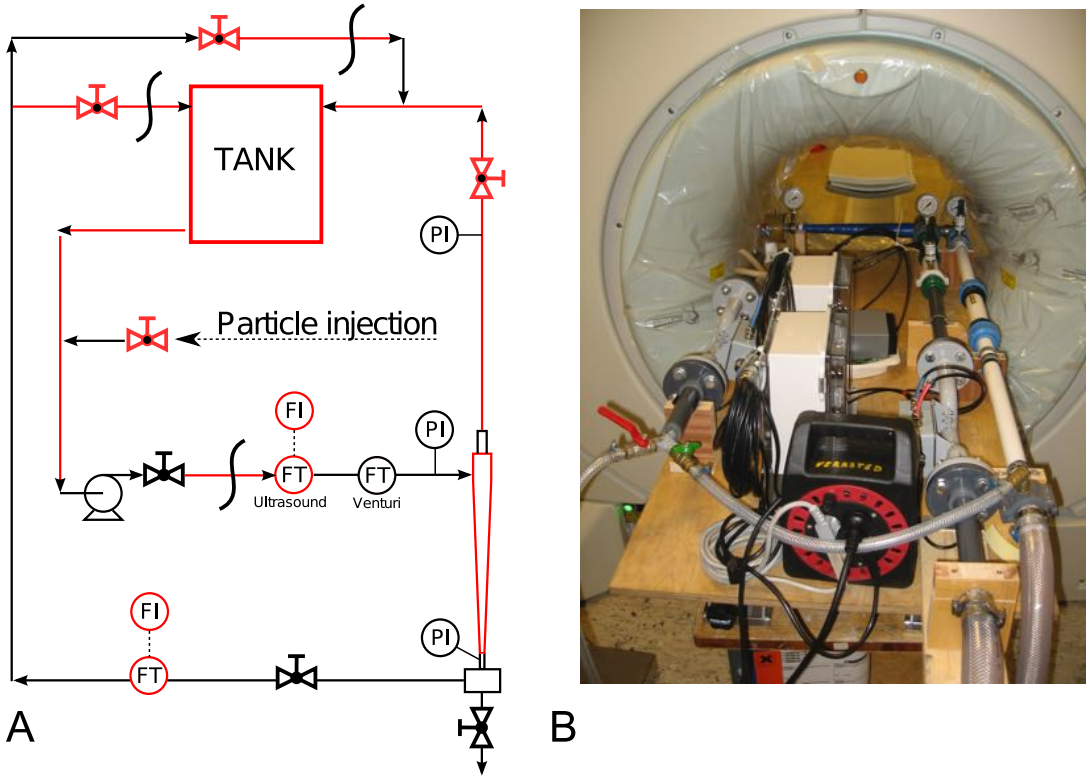

Figure 3. The experimental rig. A) Diagram showing the valving, the holding tank and the cyclone with the underflow provision. PI: pressure indicator. FI: flow indicator. FT: flow transmitter. B) Photo showing the rig installed in the PET scanner.

The experiments were performed at Haukeland University Hospital, the activation of the resin particles was also done there. A number of particles were activated before each experiment was started. The flow loop was test run to detect any leakage and to verify that it was working as designed. After testing, the rig was moved to the location of the PET scanner and placed in the scanner FOV. The flow loop was started and flow rate and underflow ratio were tuned to the desired values for each experiment. Then a particle was injected by the use of a syringe upstream of the pump at the same time as the scanner is set to start logging. The logging was continued for 90 seconds. Then the flow loop was taken out of the scanner and liquid was extracted from the collection chamber until the particles were recovered. This procedure was followed for the experiments in which the particle flowed to the collection chamber. In the experiments where the particle was not collected in the collection chamber and instead transported back to the holding tank, the logging time was increased to 120 seconds to have more particles running through the cyclone in each experiment and have a better chance of logging an individual particle moving through the cyclone without interference from any other tracer particle.

The tracer particles used were strong anion-exchange beads, Amberlyst A26 Hydroxide Form (Acros Organics). The particle size was measured with microscopy to be 430 μm, with a standard deviation of 56 μm The envelope density of the particles immersed in water was determined by settling experiments to be between 1080 and 1120 kg/m^3. This means that the particles will have the the same Stokes number, $\mathrm{Stk} \equiv \frac{(\rho_p - \rho) d_p^2}{18\mu} \frac{v_{\mathrm{in}}}{D}$ as sand particles (density $\rho_p = 2700$ kg/m^3) of diameter $d_p = 104$ μm in water, and therefore behave in the same way in the cyclone as such

sand particles. When 'tracer particle' is mentioned in this article, it is a particle with these properties. The dynamic response time of the tracer particle in water, $\frac{(\rho_p-\rho_w)*D^2}{\mu_w}$ is 0.018 s, which probably means that the turbulent dispersion of the particle is somewhat reduced, but it should not be significant compared to the mean motion or the particles' behaviour in the region of the end of the vortex. Transient effects should be revealed in both the numerical simulations and in the PEPT experiments. In the higher viscosity fluids the response time will be shorter.

A sand particle in water of 104 μm is a rather small particle, still considerably larger than the cut-size of the cyclone, but rather small in the distribution of sand particles that will be charged to the cyclone. The low relative density of the tracer particle ensures that it behaves in the same way in the cyclone as a typical sand particle that the cyclones would normally need to separate.

The experiments carried out are listed in Table1. The Reynolds number, $\mathrm{Re} \equiv \frac{\rho v D}{\mu}$, depending on viscosity, μ, density, ρ, velocity of the flow, v, and on the diameter of the cyclone body, D, can be calculated as listed in ref [31]. Alginate was chosen as a viscosity modifier, since this turned out to be the best way of modifying the fluid viscosity keeping all else constant. Alginate did give rise to slightly non-Newtonian behaviour, but this was not enough to cause any concern.

Table 1. List of the experiments carried out

Fluid	Flow rate [m^3/hr]	% underflow
Salt soln	3.4	5
Water	3.4	0
Water	3.4	5
Water	3.4	10
Water	3.4	20
Water	2	0
Water	1	0
Alginate 20 cP	3.4	5
Alginate 15 cP	3.4	5
Alginate 10 cP	3.4	5
Alginate 5 cP	3.4	5

4. Results and Discussion

4.1. The fluid flow pattern

Some PEPT experiments were performed to study the fluid flow pattern using a tracer particle with neutral density relative to the fluid. To match the density of the particle, salt was added to the water, since it was not practical to tune the density of the radioactive particle to match that of water. The drawback of this is that the ^{18}F on the tracer particle will leach into the fluid. It was nevertheless possible to obtain a number of useful tracks indicating the flow pattern of the fluid in the cyclone. In the absence of a free surface or stratification in the flow, Reynolds number similarity should ensure dynamic similarity in the cyclone, the fluid flow pattern should therefore not be affected by the density of the fluid except through the Reynolds number, and this is only weakly affected by the slight change in density that is involved here (see also Section 4.3). Some of these tracks are shown in Figure 4A, and may be compared with the streamlines for the fluid flow resulting from CFD simulations shown in Figure 4B. In accordance with the operating conditions a neutral density particle should leave the cyclone through the fluid outlet 95% of the times and the particle outlet at the bottom of the cyclone 5% of the times. It is clear that the fluid streamlines in the CFD simulations agree with the tracks in the PEPT experiments

and that the streamlines and the tracks are consistent with what would be expected on basis of the operating conditions. The streamlines shown in this paper are snapshots of the turbulent flow, which is filtered with the spatial LES filter and therefore does not reflect the fine-scale turbulence.

The experiments show that most of the tracer particles moving from the outer part of the vortex with downwards flow to the inner part with upwards flow on their way to the fluid outlet do so in the upper part of the cyclone, and the flow there is therefore the most important in determining the cyclone separation efficiency.

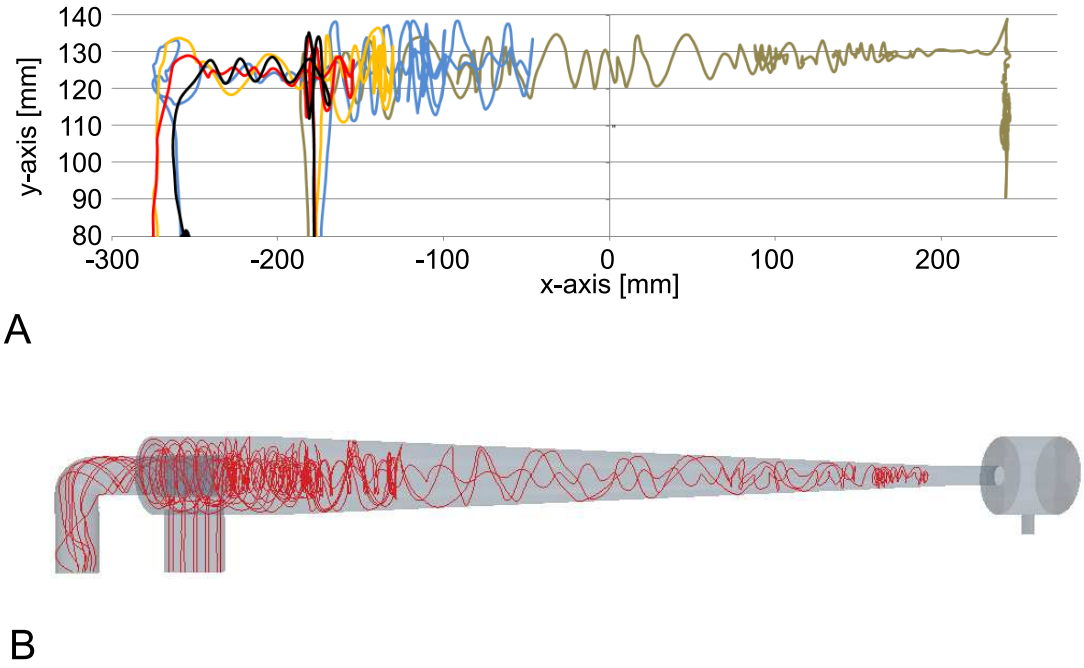

Figure 4. A) PEPT tracks of neutral density particles in the cyclone, the tracks from the different tracer particle passes have been given different colours. B) Streamlines for the fluid flow in the cyclone under the same operating conditions. Flowrate: 3.4 m^3/hr, underflow: 5%.

In the rest of the work presented in this paper the comparison between experiment and CFD will be on basis of the movement of particles that are not neutral density but have the properties described above for the tracer particles, which will be tracked by PEPT experimentally and Lagrangian tracking in the CFD simulations.

4.2. Effect of underflow

Withdrawing a stream from the bottom of the cyclone is known to often have a positive effect on the separation efficiency, at the cost of the separated particles still being obtained in an, albeit much more concentrated, fluid stream, which then has to be treated further, perhaps in a filter installation, before the particles are obtained fully separated. Underflow is often used in cyclones operating on liquids and more rarely on cyclones operating on gases. The simulations and experiments described in this section will show the important effect underflow may have on the fluid and particle flow patterns in cyclones. Figure 5 shows tracks of a tracer particle with PEPT and with CFD. Excellent agreement between PEPT and CFD is seen, even with regards to the instability in the bottom of the cyclone, which is caused by the so-called 'end of the vortex', where the vortex core bends to the cyclone wall and rotates (precesses) at a more or less

fixed axial position, which in turn causes the particle to flow in an irregular pattern, having a residence time much longer in this region than in the upper part of the cyclone, something that can clearly lead to clogging of the cyclone if the particle concentration is high. The simulations reflect correctly not only the presence of the instability under these same conditions conditions as the experiments, but even the approximate position of it. The vortex end can also lead to wear of the cyclone wall in consequence of the particles' prolonged residence time. In gas cyclones it has even been known to lead to failure with the part of the cyclone under this position falling off.

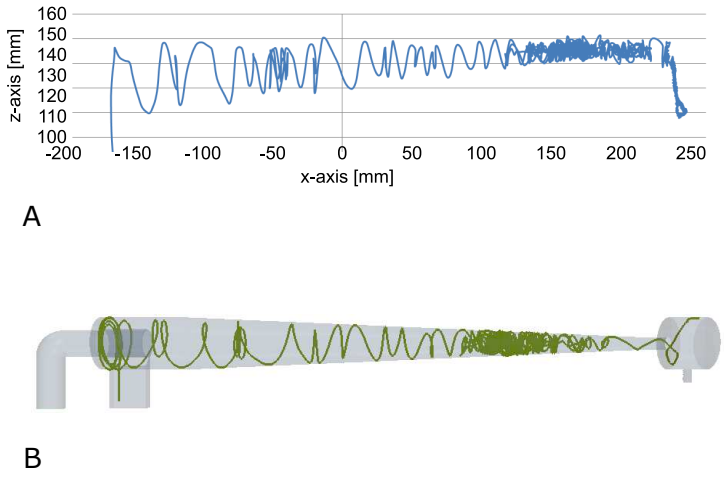

Figure 5. Experimental (A) and CFD (B) tracks of a tracer particle in the cyclone with the underflow closed. Flowrate: 3.4 m^3/hr, underflow 0%.

The pressure distribution in a plane containing the cyclone axis in the CFD simulation shown in Figure 6A confirms that the vortex motion ends at a given position in the separation space, and under this position is much weaker consistent with the idea of the vortex 'ending' at this position. A similar picture can be seen in the pressure profile in Figure 10B later in this paper. There, at the higher flow, a 'secondary vortex' under the main vortex end, described and discussed in ref [50], but not shown explicitly till now, can be distinguished under the position of the vortex end. Under the vortex end the isosurface of zero axial velocity is also less visible, as can be seen in Figure 6B.

Drawing even only a little underflow has a strong effect on this behaviour of the fluid and the particle in the bottom of the cyclone. Figure 7 shows PEPT and CFD tracks for a tracer particle with 5% underflow. The passage of the particle through the cyclone is seen to be much smoother and the severe disturbance in the bottom of the cyclone as shown in Figure 5 has completely disappeared. The agreement between PEPT and CFD is seen to be very good also in this case, confirming that the LES simulations reflect correctly also the effect of underflow on the fluid and particle flow patterns.

The pressure profile and the zero axial velocity isosurface shown in Figure 8 A and B confirm the effect seen in Figure 7 that the underflow has the effect of eliminating the end-of-vortex effects in the cyclone.

4.3. Effect of fluid flow rate

It is interesting to know if the fluid flow rate through the cyclone, and therefore the cyclone Reynolds number, has an effect on the flow pattern in the cyclone. It is normally assumed that there is no such effect, or that the effect is only weak.

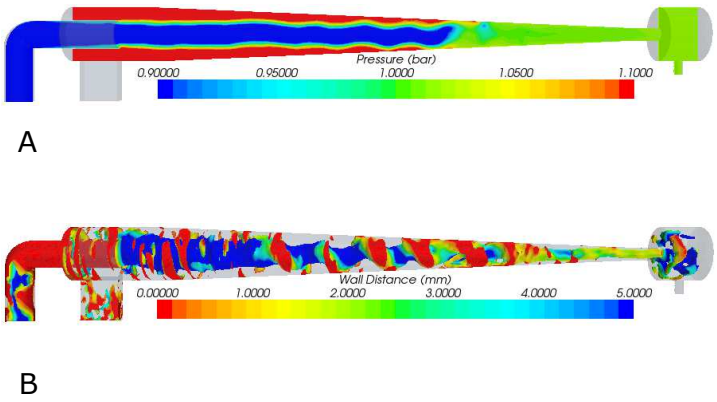

Figure 6. CFD snapshots showing A) the static pressure in a section of the cyclone containing the axis and B) isosurface of zero axial velocity coloured according to the distance from the cyclone wall. Flowrate: 3.4 m^3/hr, underflow: 0%.

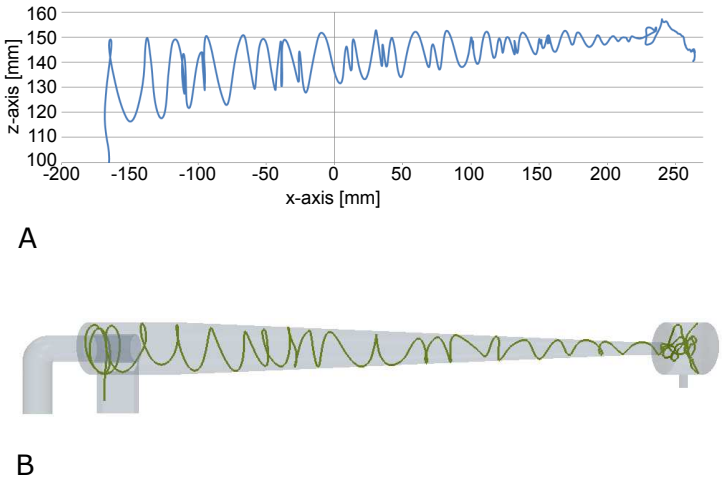

Figure 7. Experimental (A) and CFD (B) tracks of a tracer particle in the cyclone with 5% underflow. Flowrate: 3.4 m^3/hr, underflow 5%.

Figure 9 shows PEPT and CFD results from a case with low fluid flowrate through the cyclone. Some discrepancy between the experiment and CFD can be seen in this case, although both simulations and PEPT tracks indicate some instabilities near the transition from cylindrical to conical and also low in the cyclone separation space close to the particle outlet. The particle path through the cyclone is more disturbed in the experiment than in the CFD.

It is interesting the compare the CFD results with an equivalent case where the fluid flowrate is high. Figure 10 shows such a case. It appears from the static pressure distribution that the vortex is longer in the case with the low flow, this agrees well with the particle flow pattern which shows that the particle passes through the cyclone to the dust outlet relatively unhindered, but should be taken with a grain of salt since, in this respect, the CFD simulation does not agree well with the experiment.

In Figure 9 the isosurface of zero velocity is seen to be scattered to some extent due to the image representing a snapshot of an LES simulation, but a continuous surface with blue

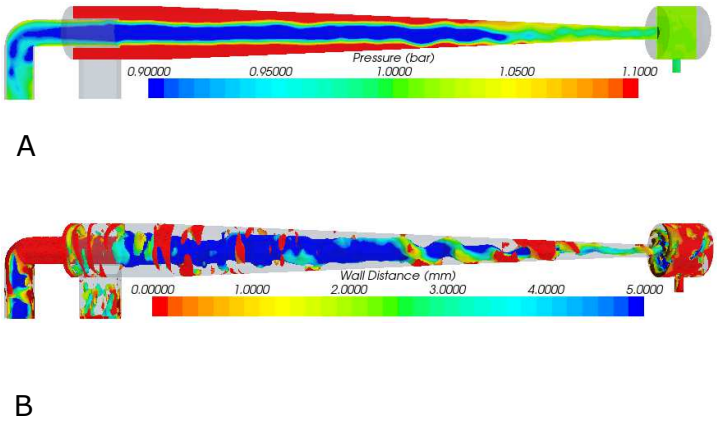

Figure 8. CFD snapshots showing A) the static pressure in a section of the cyclone containing the axis and B) isosurface of zero axial velocity coloured according to the distance from the cyclone wall. Flowrate: 3.4 m^3/hr, underflow: 5%.

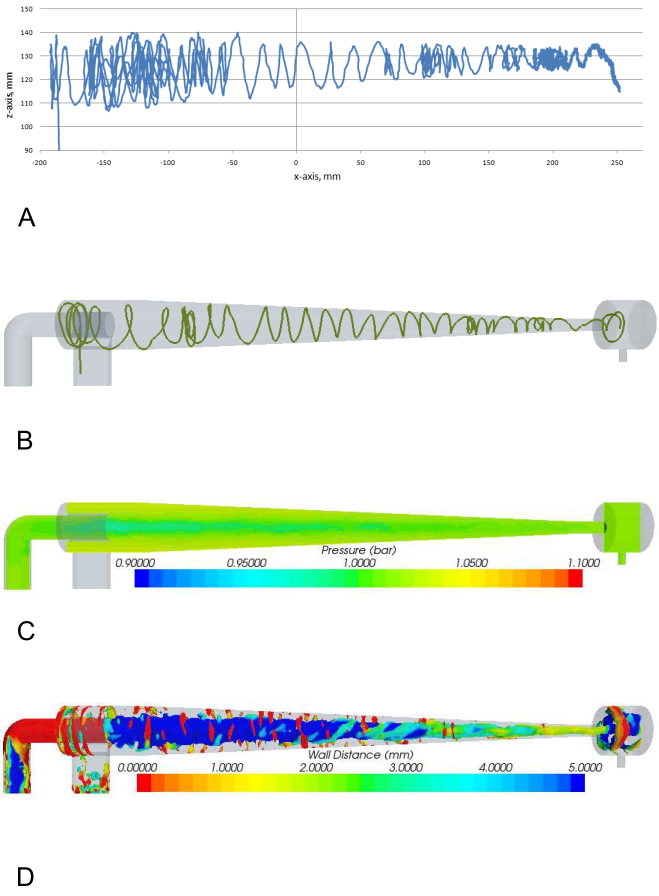

Figure 9. CFD simulations and PEPT tracks of a tracer particle in a cyclone with reduced fluid flowrate. A) PEPT tracks of tracer particle. B) Lagrangian tracks of a tracer particle in a cyclone with the same geometry and operating conditions. C) Pressure distribution in the cyclone by CFD. D) Isosurface for an axial fluid velocity of zero, coloured according to the distance from the cyclone wall. Flowrate: 1.0 m^3/hr, underflow: 0%.

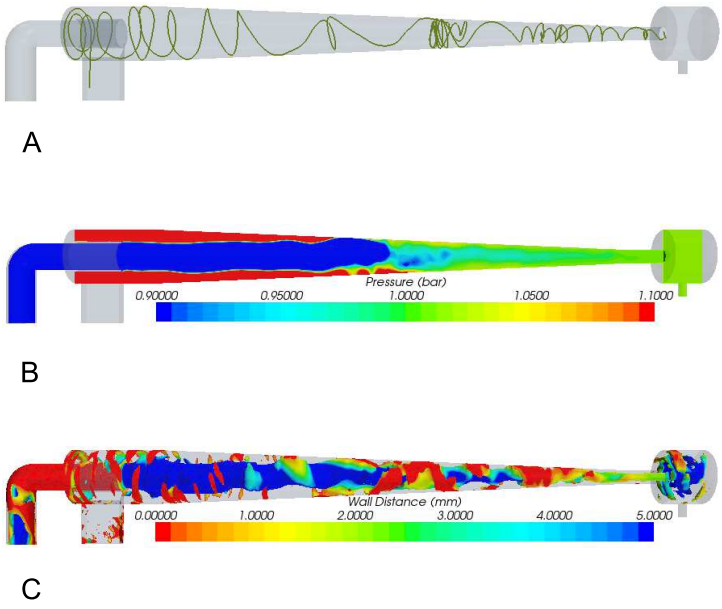

Figure 10. CFD simulations of the flow in a cyclone with high fluid flowrate. A) Lagrangian tracks of a tracer particle. B) Pressure distribution in the cyclone by CFD. C) Isosurface for the axial fluid velocity of zero, coloured according to the distance from the cyclone wall. Flowrate: 7.4 m^3/hr, underflow: 0%.

colour is seen under the fluid outlet. This surface roughly forms a cylinder under the vortex finder wall, but it seems to contract in the radial direction when moving down in the cyclone, maintaining the blue colour, indicating that the surface of zero axial velocity does, in the conical part this cyclone with a long conical section, form a 'mantle' as assumed by some as mentioned in Section 1.1. In Figure 10 the surface is seen to be less stable, indicating that the vortex becomes unstable in the lower part of the cyclone at this high flowrate, a flowrate giving rise to an inlet velocity so high that it is rarely used in practise in cyclones operating on liquids.

4.4. Effect of fluid viscosity

The effect of fluid viscosity on the separation efficiency of the cyclone has been investigated in details in a separate subproject using a separate experimental rig. This is reported elsewhere [51] and experimental results for other aspects of the effect of viscosity on the fluid flow pattern have been discussed in ref [49]. Here the focus is on CFD results, verified by PEPT results, showing the effect of fluid viscosity on the flow patterns of the fluid and the tracer particle, particularly in the bottom of the cyclone.

Figure 11A shows the pressure drop over the cyclone as a function of the viscosity of the fluid flowing in the cyclone. This confirms the, intuitively somewhat surprising, result that the pressure drop decreases with increasing viscosity in a cyclone. This phenomenon, the reason for it, and the related effect that the pressure drop in cyclones decreases with increasing wall roughness, are discussed in ref [50]. It is a consequence of a weaker swirl in the cyclone caused by increasing wall friction in the cyclone body. Figure 11B shows the pressure drop over the cyclone as a function of the liquid (water) flowrate. The pressure drop should be proportional to the square of the liquid flowrate, which is indicated by the dashed curve, and the results bear this out. The numerical results generally agreed with the experimental ones to within around 10%, which is acceptable in view of the difficulties involved in measuring the pressure drop

experimentally due to the residual swirl present in the vortex finder [50].

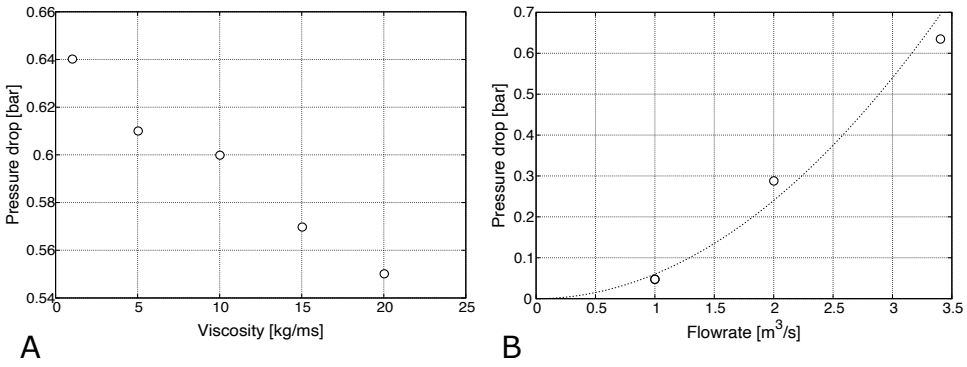

Figure 11. A) Numerical results for the pressure drop over the cyclone as function of the viscosity of the fluid. B) Numerical results for the pressure drop over the cyclone as a function of the liquid (water) flowrate.

Figure 12 shows the static pressure distribution for a CFD simulation with a flowrate of 3.4 m^3/s and a fluid of high viscosity (15 cP). The low-pressure vortex core is much less evident than for the same flow with water, an indication of the less strong vortex motion when the cyclone acts on fluids with high viscosity.

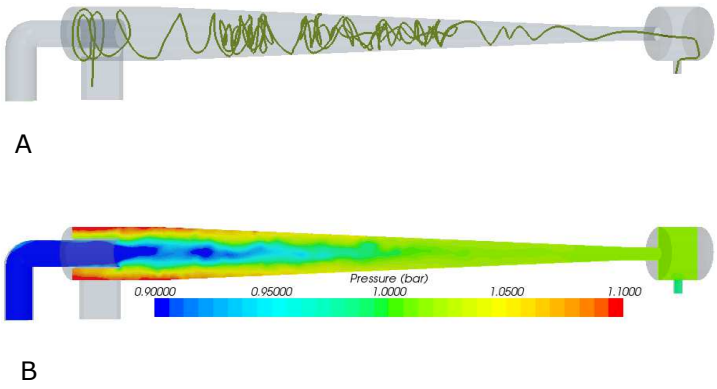

Figure 12. (B) CFD simulation of the static pressure profile when the cyclone is working on a liquid of high viscosity. Comparing with the earlier figures with the same fluid flowrate it is evident that the swirl is weaker in this case giving rise to a less evident core of low static pressure. The PEPT track shown in (A) is consistent with this, showing that the particle track is irregular in the vortex that is too weak to centrifuge the particle out into the outer part of the vortex efficiently.

4.5. Effect of a modified inlet

It is often thought that a dual inlet will lead to more axisymmetric flow in the cyclone and therefore stabilise the vortex motion in the cyclone. To test this, such a configuration was made for the CFD simulations, the height of the inlets were reduced so that the total inlet area was the same as for the single-inlet cyclone, and the results are therefore directly comparable with the

simulations for the single-inlet cyclone at the same flowrate. The geometry and the simulation results are shown in Figure 13. The flow pattern can be seen to be very similar to that in the single-inlet cyclone, and the particle path confirms the presence of the 'end of the vortex' in the separation space, causing a disturbance in the particle transport to the particle outlet.

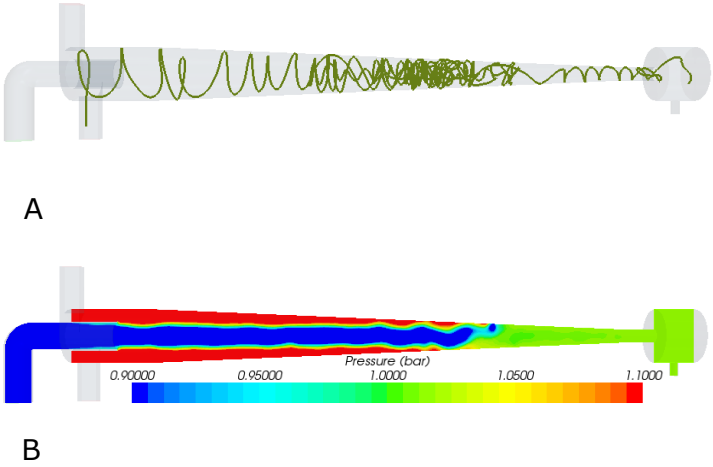

Figure 13. CFD simulations of hydrocyclone with two inlets. A) Pathlines of a particle. B) Distribution of static pressure in a plane containing the cyclone axis.

Lately increasing interest has been paid to the option of angling the cyclone inlet downwards with the aim of enhancing the downward flow in the outer part of the vortex and stabilise the vortex flow in the cyclone separation space and also to reduce the lip-leakage flow short-circuiting the cyclone [26, 52]. In order to add an unbiased assessment of the merits of such a design modification to the published literature, some simulations were performed with this configuration. Also in this case the inlets were configured so that the total inlet areas was equal to the inlet area in the single-inlet cyclone. The geometry and the results of the simulations are shown in Figure 14.

Also here the flow pattern low in the cyclone is seen to be more or less unaffected by the configuration of the inlet. A detailed study of the flows showed that this inlet configuration does lead to a reduction of the lip-leakage flow and therefore to less particles short-circuiting the cyclone in this flow and a slightly increased separation efficiency.

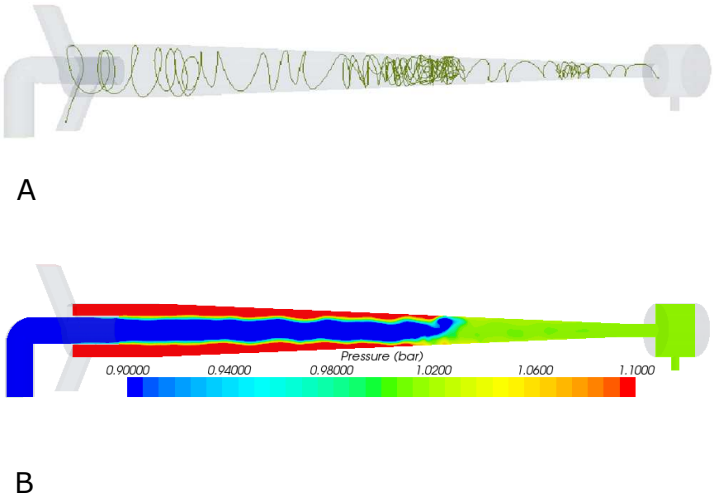

Figure 14. CFD simulations of hydrocyclone with two inlets angled downwards. A) pathlines of a particle. B) Distribution of static pressure in a plane containing the cyclone axis.

5. Conclusions

- The locus of zero axial velocity does extend from the vortex finder wall as assumed in the classical and most-used cyclone models and forms a cylindrical surface in the upper part of the cyclone as assumed in many models. Lower down it forms a conical mantle as some others hold.
- A much weaker secondary vortex below the end of the main vortex in the cyclone, as discussed in ref [48], has been demonstrated by the simulations.
- Higher viscosity fluids give rise to a weaker vortex but also to a lower pressure drop and a longer vortex.
- The classical cyclone models appear to work best at higher Reynolds numbers. At low Reynolds number the high friction factor seems to present a problem.
- A double inlet, angled downward or not, does not affect the flow low in the cyclone significantly, but the angled inlet does reduce the flow from the outer to the inner part of the vortex in the upper part of the cyclone separation space.
- LES was successful in simulating details of the flow in the cyclone.
- The position of the 'end of the vortex' is a crucial feature for the operation and design of cyclones. It is an instability that depends on the wall friction and the details of the flow pattern in the cyclone. Only recently it has been possible to model this correctly numerically using the most advanced computational techniques. The fact that this phenomenon and even the axial position at which it appears are reflected correctly in almost all of the simulations presented in this article is an important quantitative testament to the validity of the simulations.
- The only way of revealing important flow features in cyclone separators affecting the separation is Lagrangian particle tracking, showing features that point measurements, e.g. with laser Doppler anemometry (LDA) or particle image velocimetry (PIV), cannot show. The best experimental way of doing that is PEPT using an accurate cross-triangulation algorithm combined with high radioactivity on the tracer particle.

Acknowledgments
The authors gratefully acknowledge funding from the Norwegian Research Council through the PETROMAKS program. The project was established and the experimental rig built in collaboration with Aker Solutions. The authors thank the staff at Haukeland University Hospital and Siemens Healthineers for their expertise and assistance.

References

[1] Barth W 1956 *Brennstoff-Wärme-Kraft* **8, Heft 1** 1–9 (in German)
[2] Muschelknautz E 1972 *Chemie-Ing.-Techn.* **44** 63–71 (in German)
[3] Mothes H and Löffler F 1985 *Ger. Chem. Eng.* **8** 223–233
[4] Lorenz T 1996 *VDI Forschrittsberichte* **3** 1–113 (In German)
[5] Muschelknautz U 2018 *Gefahrstoffe Reinhaltung der Luft* **78** 453–465 ISSN 0949-8036
[6] Svarovsky L 2000 *Solid-Liquid Separation* 4th ed (Oxford: Butterworth-Heinemann)
[7] Wasilewski M, Brar L S and Ligus G 2020 *Separation and Purification Technology* **239**
[8] Dong S, Jiang Y, Jin R, Dong K and Wang B 2020 *Applied Mathematical Modelling* **80** 683–701 ISSN 0307–904X
[9] Zhao B, Wang D, Su Y and Wang H L 2020 *Separation and Purification Reviews* **49** 112–142 ISSN 1542-2119
[10] Nakhaei M, Lu B, Tian Y, Wang W, Dam-Johansen K and Wu H 2020 *PROCESSES* **8**
[11] Wasilewski M and Brar L S 2019 *Separation and Purification Technology* **213** 19–33 ISSN 1383-5866
[12] Wang J, Guo Y and Pan J 2019 *Powder Technology* **345** 457–467
[13] Bartz-Beielstein T, Zaefferer M and P Q C 2018 *Structural and Multidisciplinary Optimization* **58** 919–933 ISSN 1615-147X
[14] El Ashry Y, Abdelrazek A M and Elshorbagy K A 2018 *Separation Science and Technology* **53** 2500–2516 ISSN 0149-6395
[15] Wasilewski M 2017 *Separation and Purification Technology* **179** 236–247 ISSN 1383-5866
[16] Bogodage S G and Leung A Y T 2016 *Journal of Hazardous Materials* **311** 100–114 ISSN 0304-3894
[17] Singh P, Couckuyt I, Elsayed K, Deschrijver D and Dhaene T 2016 *Applied Mathematical Modelling* **40** 4248–4259 ISSN 0307-904X
[18] Gronald G and Derksen J J 2011 *Powder Technology* **205** 160–171
[19] Hoffmann A C, Vansanten A, Allen R W K and Clift R 1992 *Powder Technology* **70** 83–91
[20] Peng W M, Hoffmann A C, Dries H, Regelink M and Foo K K 2007 *AIChE Journal* **53** 589–597
[21] Chang Y F, Ilea C G, Aasen O L and Hoffmann A C 2011 *Chemical Engineering Science* **66** 4203–4211
[22] Li A, Zhu L, Wang K, Wang G and Wang Z 2020 *Powder Technology* **364** 205–217 ISSN 0032–5910
[23] Gopalakrishnan B and Prakash K A 2019 *International Journal of Advances in Engineering Sciences and Applied Mathematics* **11** 280–287
[24] Tofighian H, Amani E and Saffar-Avval M 2020 *Powder Technology* **360** 1237–1252 ISSN 0032–5910
[25] Svensen E A and Hoffmann A C 2020 *Heliyon* **6** ISSN 2405–8440
[26] Wasilewski M and Brar L S 2019 *Separation and Purification Technology* **213** 19–33 ISSN 1383–5866
[27] Parvaz F, Hosseini S H, Elsayed K and Ahmadi G 2018 *Separation and Purification Technology* **201** 223–237 ISSN 1383–5866
[28] Li G and Lu Y 2018 *Particuology* **39** 55–67 ISSN 1674–2001
[29] Huang A N, Ito K, Fukasawa T, Yoshida H, Kuo H P and Fukui K 2018 *Separation and Purification Technology* **190** 25–32 ISSN 1383–5866
[30] Mousavian S M and Najafi A F 2009 *Archive of Applied Mechanics* **79** 1033–1050
[31] Skorpen Å 2012 *Investigation of Particle Trajectories and Flow Patterns in a Hydrocyclone by Positron Emission Particle Tracking (PEPT)* (Master's thesis, The University of Bergen)
[32] Fangary Y S, Barigou M, Seville J P K and Parker D J 2000 *Chemical Engineering Science* **55** 5969–5979 ISSN 0009–2509
[33] Snieders F F, Hoffmann A C, Cheesman D, Yates J G, Stein M and Seville J P K 1999 *Powder Technology* **101** 229–239
[34] Hoomans B P B, Kuipers J A M, Salleh M A M, Stein M and Seville J P K 2001 *Powder Technology* **116** 166–177 ISSN 0032–5910
[35] Parker D J, Dijkstra A E, Martin T W and Seville J P K 1997 *Chemical Engineering Science* **52** 2011–2022 ISSN 0009–2509
[36] Bailey D L, Maisey M N, Townsend D W and Valk P E 2003 *Positron Emission Tomography: Basic Sciences and Clinical Practice* (London: Springer-Verlag)
[37] Chang Y F, Hoffmann A C and Adamsen T C H 2012 *Proceedings of the 2012 IEEE International Instrumentation and Measurement Technology Conference, I2MCT* (Graz, Austria)

[38] Sovechles J M, Boucher D, Pax R, Leadbeater T, Sasmito A P and Waters K E 2017 *Measurement Science and Technology* **28** 095402
[39] Wiggins C, Santos R and Ruggles A 2017 *Nuclear Instruments and Methods in Physics Research Section A: Accelerators, Spectrometers, Detectors and Associated Equipment* **843** 22–28
[40] Blakemore D M, Govender I, McBride A T and Mainza A N 2019 *Chemical Engineering Science* **207** 780–789
[41] Nicusan A and Windows-Yule C 2020 *Review of Scientific Instruments* **91** 013329
[42] Cole K, Buffler A, van der Meulen N, Cilliers J, Franzidis J P, Govender I, Liu C and van Heerden M 2012 *Chemical Engineering Science* **75** 235–242 ISSN 0009-2509
[43] Parker D J 2017 *Review of Scientific Instruments* **88** ISSN 0034-6748
[44] van Heerden M R, Cole K, van der Meulen N P, Franzidis J and Buffler A 2020 *Applied Radiation and Isotopes* **158** ISSN 0969-8043
[45] Boucher D, Jordens A, Sovechles J, Langlois R, Leadbeater T W, Rowson N A, Cilliers J J and Waters K E 2017 *Minerals Engineering* **100** 155–165 ISSN 0892-6875
[46] Valdesueiro D, Garcia-Trinanes P, Meesters G M H, Kreutzer M T, Gargiuli J, Leadbeater T W, Parker D J, Seville J P K and van Ommen J R 2016 *Nuclear Instruments & Methods in Physics Research Section A-Accelerators Spectrometers Detectors And Associated Equipment* **807** 108–113 ISSN 0168-9002
[47] Cole K, Buffler A, Cilliers J J, Govender I, Heng J Y Y, Liu C, Parker D J, Shah U V, van Heerden M and Fan X 2014 *Powder Technology* **263** 26–30 ISSN 0032-5910
[48] Pisarev G I, Hoffmann A C, Peng W and Dijkstra H A 2011 *Applied Mathematics and Computation* **217** 5016–5022
[49] Hoffmann A C, Skorpen Å and Chang Y F 2019 *Chemical Engineering Science* **200** 310–319
[50] Hoffmann A C and Stein L E 2007 *Gas Cyclones and Swirl Tubes, Principles, Design and Operation* 2nd ed (Berlin, Heidelberg, New York: Springer)
[51] Marthinussen S A, Chang Y F, Balakin B and Hoffmann A C 2014 *Chemical Engineering Science* **108** 169–175
[52] Borhani Jebeli M, Moridi P, Beheshti M H and Yarahmadi R 2020 *International Journal of Environmental Science and Technology* **17** 1075–1086